# Supplementary information

## Si-nanocrystal/P3HT hybrid films with a 50- and 12-fold enhancement of hole mobility and density: films prepared by successive drop casting

Daisuke Kajiya[a] and Ken-ichi Saitow*[a,b]

[a] Natural Science Center for Basic Research and Development (N-BARD), Hiroshima University, 1-3-1 Kagamiyama, Higashi-hiroshima, Hiroshima 739-8526, Japan

[b] Department of Chemistry, Graduate School of Science, Hiroshima University, 1-3-1 Kagamiyama, Higashi-hiroshima, Hiroshima 739-8526, Japan

*Corresponding Author: saitow@hiroshima-u.ac.jp

**Table S1.** High-efficiency hybrid and organic photovoltaics. PCE: power conversion efficiency.

| Type | Materials | PCE(%) | Reference |
|---|---|---|---|
| **Hybrid inorganic and organic photovoltaic** | | | |
| Inorganic nanomaterial | **PDTPBT/$PbS_{0.4}Se_{0.6}$** | **5.5** | 1 |
| and organic polymer | P3HT/CdTe | 4.3 | 2 |
| | P3HT/PCBM/$Cu_2S$ | 4.3 | 3 |
| | PTB7/Si | 3.6 | 4 |
| | PCPDTBT/CdSe | 3.13 | 5 |
| | P3HT/GaAs | 2.36 | 6 |
| | P3HT/Si | 2.2 | 7 |
| | P3HT/CdS | 4.1 | 8 |
| | P3HT/PCBM/$CuInS_2$ | 1.6 | 9 |
| | P3HT/mesoporous-$TiO_2$ | 2.8 | 10 |
| | P3HT/$TiO_2$ | 2.2 | 11 |
| | P3HT/ZnO | 2 | 12 |
| | P3HT/PbS | 1.98 | 13 |
| | P3HT/$Bi_2S_3$ | 1.01 | 14 |
| Perovskite | perovskite/polytriarylamine | 20 | 15 |
| Dye-sensitized | Dye coded SM315 | 13 | 16 |
| | Indenoperylene Dye | 12.5 | 17 |
| Bilayer of inorganic and organic | Crystal-Si/PEDOT:PSS | 13.6 | 18 |
| | Amorphous-Si/Polymer, tandem | 11.7 | 19 |
| | Poly-Si/PEDOT:PSS | 9.7 | 20 |
| Quantum Dot | PbS, pyramid structure | 9.2 | 21 |
| | PbS, EDT at interface | 8.5 | 22 |
| **All-organic photovoltaics** | | | |
| Polymer and small molecules | Triple junction [a] | **11** | 23 |
| | Double junction (Homo) [c] | **11.3** | 24 |
| | Double junction (Hetero) [c] | 10.6 | 25 |
| | Single junction, ternary [b] | **10.5** | 26 |
| | Single junction (PNTz4T&PCBM) | 10.1 | 27 |
| | PTB7:PCBM | 8.7 | 28 |
| Oligomer | oligothiophene | 10.08 | 29 |
| Small molecule | Tandem | 10.1 | 30 |
| | Porphyrin derivative | 8.08 | 31 |

[a] P3HT:ICBA/PTB7-Th:PCBM/PDTP-DFBT:PCBM, [b] PTB7-Th:PCBM:*p*-DTS$(FBTTH_2)_2$

[c] Homo: PTB7-Th:PCBM., Hetero: P3HT:ICBA/PDTP-DFBT:PCBM

**Table S2.** Methods used for the preparation of Si-NC/P3HT hybrid films in the present and previous[32] studies

| Methods | Present study | Previous study |
|---|---|---|
| Si-NCs synthesis | pulsed laser ablation | plasma synthesis |
| Si-NC diameter | 5, 8, 11, 14 nm | 3-5 nm |
| Si-NC surface | H, SiOx, and CHx | H |
| P3HT material | Rieke Metals, 4002-E | Rieke Metals, 4002-E |
| regioregularity | 91-94% | 91-94% |
| solvent | chlorobenzene (CB) | 1,2-dichlorobenzene (DCB) |
| film preparation method | drop cast (successive) | spin coat |
| film thichness | 5－13 μm | 150 nm |
| annealing condition | 120 $^{o}$C for 30 min. | 150 $^{o}$C for 120 min. |
| Si-NCs concentration in film | 0－60 wt% | 50 wt% |
| hole mobility measurement | time-of-flight (TOF) | space-charge-limited current (SCLC) |
| transport direction of carriers | normal to the substrate | normal to the substrate |

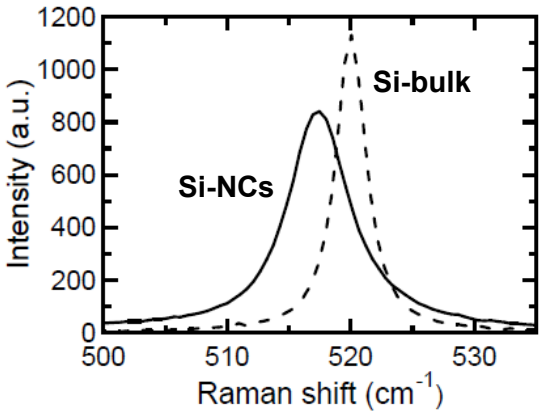


**Fig. S1.** Raman spectra of Si-NCs fabricated by pulsed laser ablation (solid line) and for bulk Si crystals (dashed line). The Raman spectra were measured using a Raman microscope spectrometer (Horiba Jobin Yvon, LabRam HR800) with an $Ar^+$ laser (Melles Griot, 543-AP-A01) at an excitation wavelength of 514.5 nm and a CCD detector. The Raman band at 520 $cm^{-1}$ is assigned to the Raman optical phonon mode of crystalline Si.[33] The Si-NCs were not amorphous, but were confirmed to be crystalline silicon. The peak frequencies of the Raman spectra for the Si-NCs are 1–5 $cm^{-1}$ lower than that of bulk Si. This frequency shift has been observed in nanostructured Si.[34] According to the correlation length model,[35] a low-frequency shift of 1–5 $cm^{-1}$ corresponds to a diameter of 5–15 nm, which is in agreement with the size obtained by DLS measurements (Fig. 8).

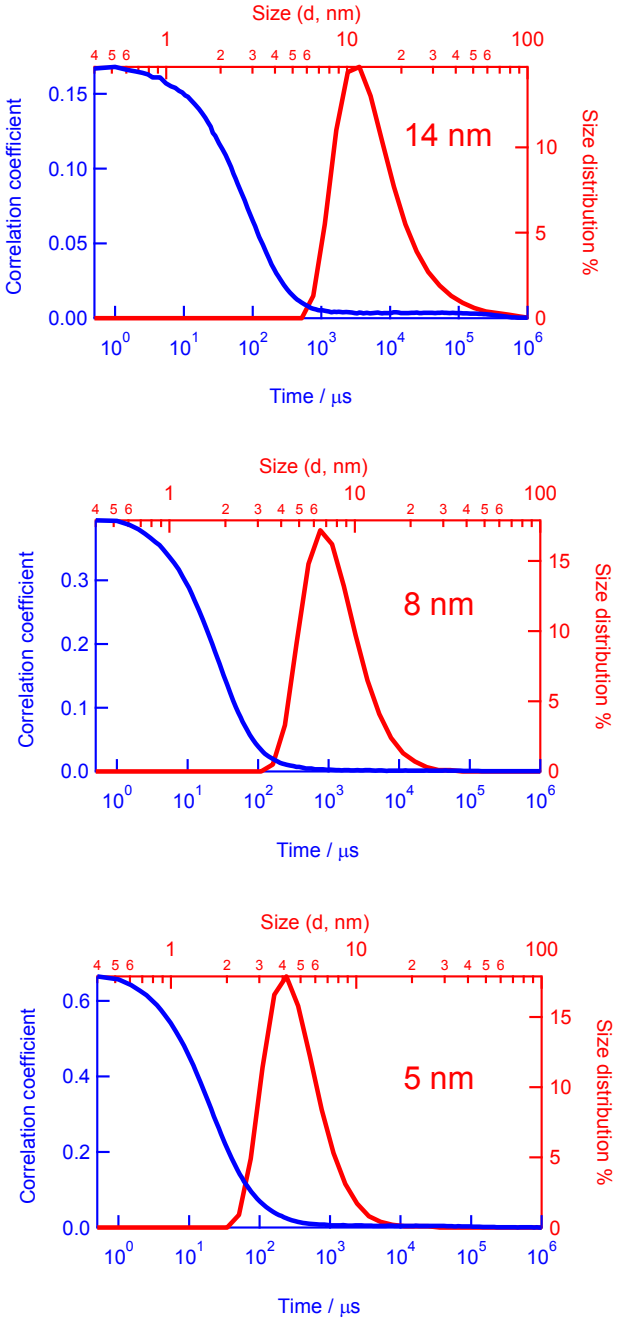


**Fig. S2.** Time-correlation function and size distribution function obtained from DLS measurements. Blue and red lines are time-correlation function and size distribution of Si-NCs obtained from the correlation function, respectively. The 5 nm Si-NCs was generated by PLA of a Si wafer immersed in ethanol. The other size Si-NCs were generated by PLA of a Si wafer immersed in 2-propanol and the different size Si-NCs were generated by changing the pulsed laser energy of the PLA.

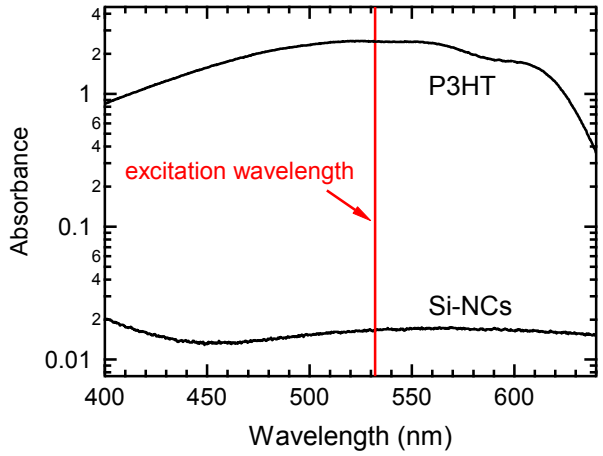


**Fig. S3.** Absorption spectra of P3HT film (dashed line) and Si-NCs film (solid line). Dotted line represents the wavelength of 532 nm that corresponds to the excitation wavelength of TOF measurement.

Fig. S3 shows the absorption spectra of P3HT and Si-NCs films. The thicknesses of P3HT film and Si-NCs film were prepared as 380 nm and 130 nm, respectively, because these values correspond to the composition ratios of hybrid film of P3HT (75wt%) and Si-NCs (25wt%). As shown in Fig. S3, almost light (> 99%) is absorbed by P3HT at the excitation wavelength of 532 nm, at which all TOF measurements are carried out. Namely, the light absorption of Si-NCs is negligible, i.e. the light absorption of P3HT is 150 times larger than that of Si-NCs.

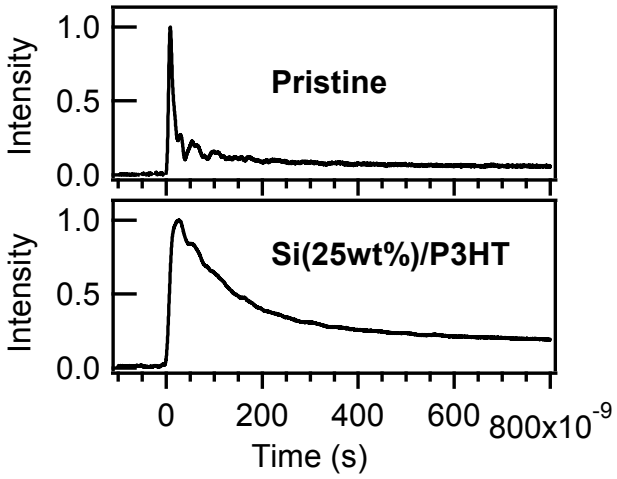


**Fig. S4.** Fast decay components of TOF signals for the pristine and hybrid films, measured at a pulsed energy of 0.5 μJ/pulse, a load resistance of 50 Ω, and using the 8 nm Si-NCs. The slower decay for the hybrid film indicates the lower hole-electron recombination.

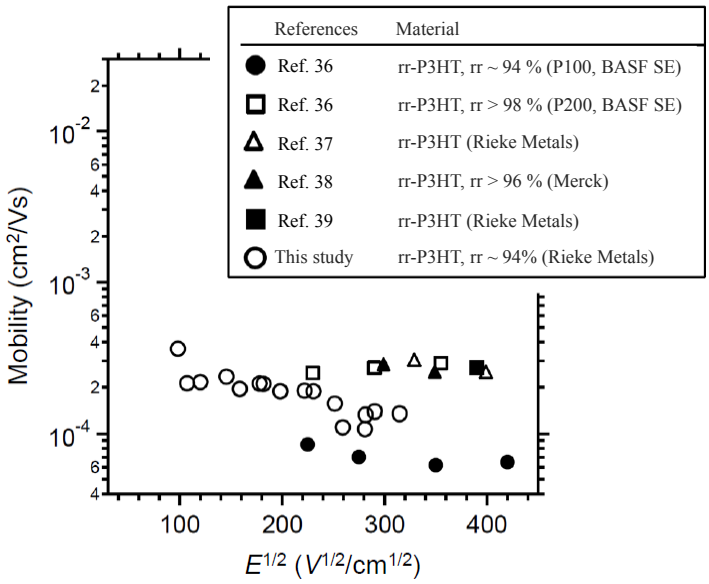


**Fig. S5.** Hole mobilities of pristine P3HT films in the present and previous[36–39] studies obtained by TOF measurements. The mobility obtained in the present study is almost equivalent to that previously reported; the hole mobility changes with the electric field, and this phenomenon has been observed in organic materials with disordered materials such as organic polymers.[37,39]

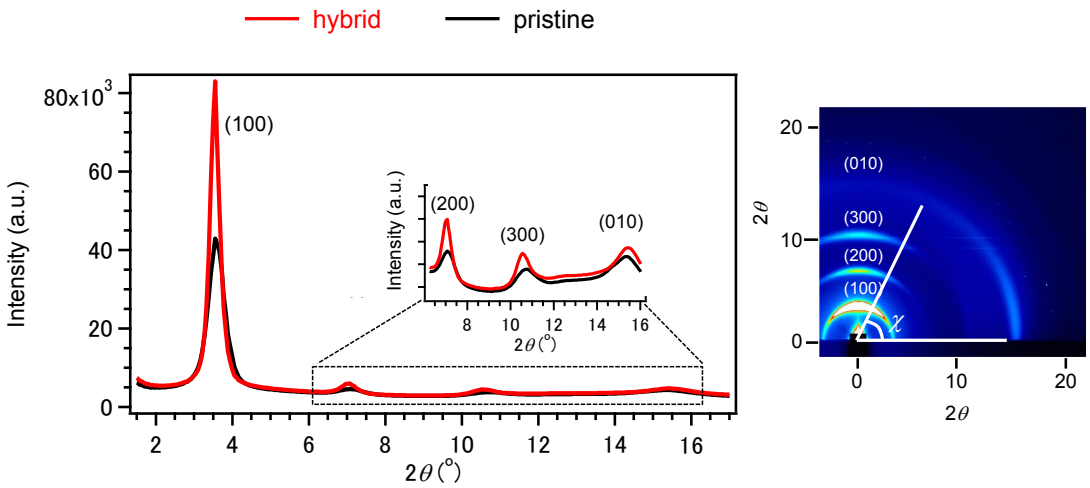


**Fig. S6.** X-ray diffraction patterns of pristine (black) and hybrid (red) films. The right figure shows the definition of $\chi$ angle in a typical 2-D image.

We measured the grazing incidence X-ray diffraction (XRD) patterns of the films to investigate the P3HT crystallinity between the pristine and hybrid (25wt% Si-NCs, 8 nm) films. The XRD measurement was conducted at the SPring-8 BL19B2 beamline with an X-ray energy of 12.39 keV ($\lambda$ = 1 Å). The X-ray was irradiated at an incident angle of 0.12° and the scattered X-ray was recorded using a 2-D image detector (Dectris, Pilatus 300K). The pristine and hybrid films were prepared by the same as the films used for the TOF measurements. The intensity of the incident X-ray was constant during all the measurement.

Fig. S6 shows the XRD patterns of pristine (black) and hybrid (red) films, whose data are obtained from the integrated intensity of $\chi$ = 0 to 90. The (100), (200), (300), and (010) peaks of P3HT crystalline are observed in the both films. For the hybrid film, the diffraction intensity becomes stronger and its profile becomes sharper. This indicates that the crystallinity of P3HT in the hybrid film is higher than that in the pristine film. From the line width of the diffraction (100), the crystallite sizes were estimated as 11 nm (pristine) and 17 nm (hybrid) using the Scherrer formula. The increase of crystallinity in the hybrid film was also observed from the viewpoint of lamellar structure. That is, both the decrease of intermolecular π–π distance (higher-angle shifting of (010)) and the increase of intermolecular lamellar spacing (lower-angle shifting of (100)) are observed. Such a π–π shrinkage together with an expansion of lamellar spacing is recognized as an increase of crystallization.[40] Thus, the results of XRD measurements revealed that the P3HT in hybrid film is more crystalline than that in the pristine film.

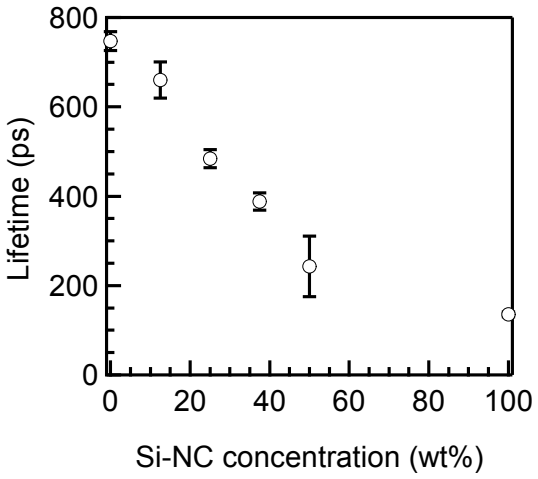


**Fig. S7.** PL lifetime of the Si-NC(8 nm)/P3HT hybrid film as a function of Si-NC concentration.

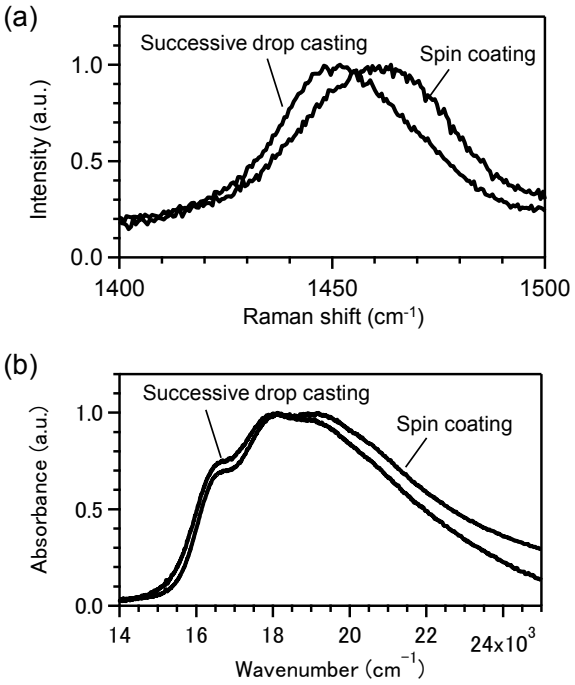


**Fig. S8.** (a) Raman spectra of the C=C stretching modes of P3HT in the hybrid films (25 wt%, 8 nm) prepared by the successive drop casting (solid line) and the spin coating (dashed line) with the film thickness of ca. 150 nm. The successive drop casting film with ca. 150 nm thickness was prepared by spreading the dropped solution slowly on the substrate. The peak frequency of the successive drop film is the lower than the spin coating film. This result indicates that the successive drop casting increases P3HT aggregations, which are established by many P3HT-monomer molecules with a highly planar backbone structure.[41–43] (b) Electronic absorption spectra of the hybrid films with the film thickness of ca. 150 nm. The lower-energy component of the spectrum of the successive drop film is larger than that in the spin coating film, indicating that the successive drop casting increases P3HT aggregations.[44,45]

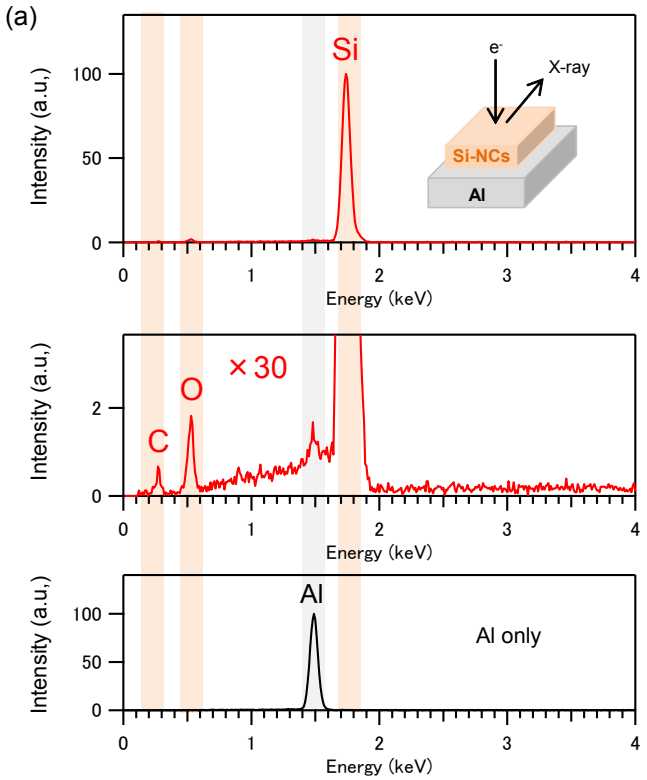


(b)

Experimental results of EDX measurements

| atomic % | Si | O | C |
|---|---|---|---|
| | 82 | 10 | 8 |
| | 82 | 10 | 8 |
| | 78 | 15 | 7 |
| | 88 | 6 | 6 |
| | 73 | 11 | 16 |
| | 82 | 8 | 10 |
| average | 81 | 10 | 9 |

**19 %**

(c)

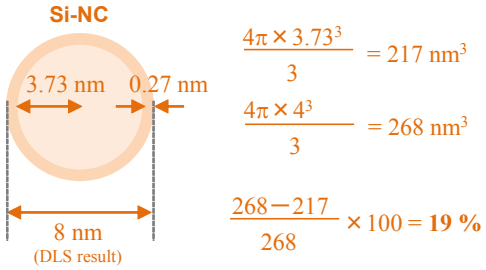


**Fig. S9.** SEM/EDS result. (a) Typical EDS spectrum of Si-NCs prepared on Al (top) and its expanded data (middle), and the spectrum of Al only (bottom). (b) Relative ratio of Si, O, and C atoms, obtained from the analysis of EDS spectra. 6 measurement data and average data are listed. (c) Estimation of the passivation thickness. The DLS result is shown in Fig. 8.

Fig. S9(a) shows the typical data of energy dispersive X-ray spectroscopy (EDS) of Si-NCs, which is measured with a SEM (Hitachi High-Technologies, S-3400N) operated at an acceleration voltage of 20 kV and equipped with an EDS system (EDAX, Genesis). The relative ratios of Si, O, and C atoms obtained from the spectra are listed in the table as S9(b). The Si-NCs is composed of Si 81%, O 10%, and C 9%. The Si-NCs diameter is measured as 8 nm by the dynamic light scattering. Using the relative ratio of element, the Si-NC size, and the spherical shape of Si-NC, it can be considered that the structure of Si-NC is the core radius of 3.73 nm and the passivation thickness of 0.27 nm, as illustrated in Fig. S9(c). The 0.27 nm thickness corresponds to single passivation layer, because typical Si-O bond length is 0.16 nm and the van der Waals radius of O atom is ca. 0.15 nm.[46]

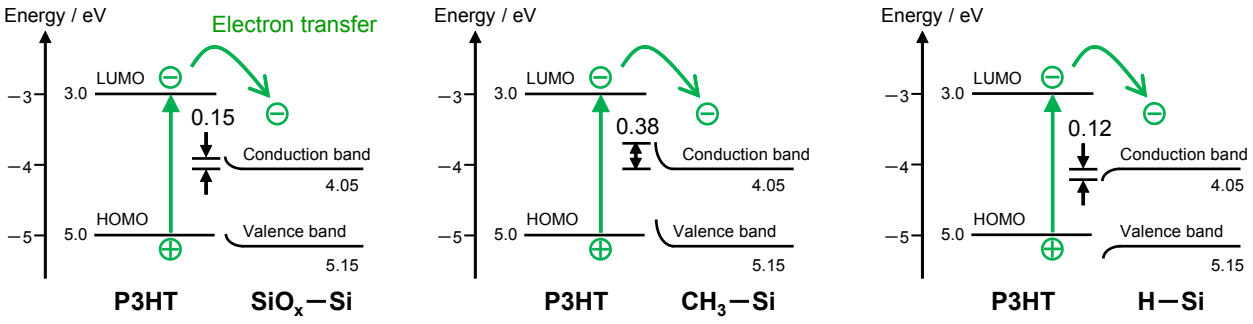


**Fig. S10.** The energy diagrams of the passivated Si and P3HT after refs. 47 and 48.

The energy diagrams of Si passivated by single $SiO_x$, $CH_x$, and H have been reported,[47,48] as shown in Fig. S10. Conduction-band energies are changed by 0.15, 0.38, and -0.12 eV by $SiO_x$, $CH_x$, H, respectively. There is no barrier for the electron transfer from P3HT to Si. Thus, the electron can transfer at the interface between P3HT and Si-NCs.

**Note S1. Effect of 2-propanol on the morphology and mobility of pristine P3HT film.**

During the successive drop casting process, 2-propanol was used as the dispersion solvent for the dispersion of Si-NCs. Thus, successive drop casting was conducted by drop casting the solution of Si-NCs in 2-propanol, followed by drop casting the solution of P3HT in chlorobenzene, as illustrated in Fig. 5a. The weight ratio of solvents on the ITO-coated glass substrate was 2 wt% 2-propanol and 98 wt% chlorobenzene, which was determined using an analytical balance. Here, the effects of 2-propanol on the film morphology, P3HT crystallinity, and hole mobility were investigated. P3HT films were prepared with and without 2-propanol, as illustrated in Figs. S11a and S11b. The morphology (Fig. S12) and hole mobility (Table S3) of the two films were then examined. The results indicated that the 2-propanol solvent does not affect the film morphology or hole mobility; (i) AFM images of the two films revealed the same morphology (Figs S12b and S12c) and no nanowires were observed in either film. In contrast, many P3HT nanowires were observed in the AFM image of the Si-NC/P3HT hybrid film, as shown in Fig. S12a. These results indicate that the addition of the Si-NCs results in a film with a high degree of P3HT crystallinity, while the solvent has no such effect. (ii) The mobilities of the two pristine P3HT films prepared with and without 2-propanol were almost the same (Table S3), whereas the mobility of the Si-NC/P3HT hybrid film was greater than the two pristine films. Thus, it was confirmed that the addition of Si-NCs is responsible for the enhancement of mobility in the hybrid film.

**Fig. S11.** Schematic diagrams for the preparation of pristine P3HT films.

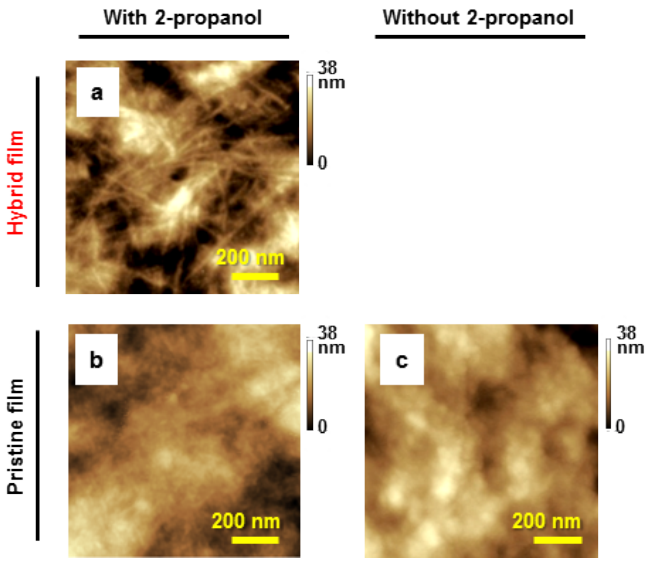


**Fig. S12.** AFM images of P3HT thin films. (a) Hybrid film (8 nm, 25 wt%) with Si-NCs prepared by successive drop casting (Fig. 5a). (b,c) Pristine films prepared by the methods shown in (b) Fig. S11a and (c) Fig. S11b. Large amounts of P3HT nanowire are evident only in the hybrid film.

**Table S3.** Mobilities of hybrid film (8 nm, 25 wt%) and pristine film. (unit: $cm^2/(V \cdot s)$)

| | With 2-propanol | Without 2-propanol |
|---|---|---|
| Hybrid film | $(9.7 \pm 1.1) \times 10^{-3}$ | — |
| Pristine film | $(2.4 \pm 0.5) \times 10^{-4}$ | $(2.0 \pm 0.2) \times 10^{-4}$ |

**Note S2. Geometrical and collected charges at the mobility measurements.**

The mobility was obtained from the equation of $\mu = d/Et$. This equation has been recognized when the geometrical charges $Q_g$ is greater than the total collection charges $Q_c$.[49,50] In the present study, it was ensured as $Q_g = 4\times10^{-9}$ C and $Q_c = 1\times10^{-10}$ C. Details are described in the following.

The $Q_g$ is expressed by the following equation:

$$Q_g = \varepsilon SV/d, \quad (1)$$

where $\varepsilon$ is the dielectric constant, $S$ is the area of electrode, $V$ is the applied voltage, and $d$ is the film thickness. Eq. (1) is obtained from $C = Q_g/V = \varepsilon S/d$, where $C$ is the capacitance. The $Q_c$ is also expressed by the following equation:

$$Q_c = \int V_{TOF}(t)R^{-1}\,dt, \quad (2)$$

where $V_{TOF}(t)$ is the voltage of TOF signal, $t$ is the time, and $R$ is the load resistance. eq. (2) is obtained from $V_{TOF}(t) = RI(t)$, where $I(t)$ is the photocurrent. For the experimental condition of the mobility measuerment, the $Q_g = 4\times10^{-9}$ C and $Q_c = 1\times10^{-10}$ C for the hybrid film, and the $Q_g = 3\times10^{-9}$ C and $Q_c = 1\times10^{-9}$ C for the pristine film. This results revealed that $Q_g$ is greater than $Q_c$. Used parameters for the calculations are listed in the following table.

**Table S4. Parameters for the calculations at the conditions of the mobility measurements.**

| | Pristine film | Hybrid film |
|---|---|---|
| $\varepsilon$ ($10^{-11}$ C$^2$/Jm) [a)] | 3.9 | 5.4 |
| $S$ (mm$^2$) | 16 | 16 |
| $V$ (V) | 48 | 48 |
| $d$ (μm) | 10 | 10 |
| $R$ (Ω) | 1000 | 50 [b)] |

[a)] $\varepsilon$ has been reported to $3.9\times10^{-11}$ C$^2$/Jm for P3HT and $10.4\times10^{-11}$ C$^2$/Jm for Si.[51,52] For the case of the hybrid film, $\varepsilon$ is obtained from the film thickness, the weight ratio ($w$) of Si and P3HT, and the densities ($\rho$) of Si and P3HT. Namely, $\varepsilon = \varepsilon_{Si}\times\{(w_{Si}/\rho_{Si})^{2/3}/[(w_{Si}/\rho_{Si})^{2/3}+(w_{P3HT}/\rho_{P3HT})^{2/3}]\}+\varepsilon_{P3HT}\times\{(w_{P3HT}/\rho_{P3HT})^{2/3}/[(w_{Si}/\rho_{Si})^{2/3}+(w_{P3HT}/\rho_{P3HT})^{2/3}]\}$, where the subscripts Si and P3HT express the Si and P3HT materials, respectively. The $w$ are 25wt% and 75wt% for Si and P3HT, respectively, and the $\rho$ are 2.3 g/cm$^3$ for Si and 1.1 g/cm$^3$ for P3HT.[46,53]

[b)] The load resistance for mobility measurement of the hybrid film was set to 50 Ω to determine the short transit time accurately with a high time resolution. The resistance for the pristine film was increased to 1 kΩ, because the transit time at 50 Ω was long and the TOF signal was too weak to be accurately detected.

**Note S3. Hole mobility of hybrid film at higher Si-NCs concentration.**

The hole mobility of hybrid film was measured by changing the Si-NCs concentration. As a result, the mobilities at Si-NCs concentrations of 25wt% and 60wt% were $9.7\times10^{-3}$ $cm^2V^{-1}s^{-1}$ and $0.2\times10^{-3}$ $cm^2V^{-1}s^{-1}$, respectively. This result elucidated that the mobility decreases by increasing Si-NCs concentration and the carriers do not transport through only Si-NCs.

**Note S4. Hole densities for the pristine and hybrid films.**

The hole density can be given by the TOF signal. Namely, the amount of holes ($Q$) is expressed by $Q = \int I(t)dt$, where $I(t)$ is the photocurrent obtained from $I(t) = V_{TOF}(t)/R$, $t$ is the time, $V_{TOF}(t)$ is the voltage observed in Fig. 3, and $R$ is the load resistance. In the present study, the $Q$ were estimated as the following. [a]

Pristine film: $(0.13\pm0.06)\times10^{-8}$ C,

Hybrid film: $(1.5\pm0.3)\times10^{-8}$ C.

The $Q$ for the hybrid film is 12 times greater than that of the pristine film. The film thicknesses of the pristine and hybrid films were the same. Accordingly, the hole density for the hybrid film was 12 times greater than that for the pristine film.

[a] Experimental conditions for the hybrid film were all the same as those for the pristine film, i.e., the pulsed energy is 0.5 μJ/pulse, the film thickness is 6 μm, the applied voltage is 51 V, and the load resistance is 1 kΩ.

**ACKNOWLEDGMENT**

XRD experiments were performed at the BL19B2 SPring-8 with the approval of the Japan Synchrotron Radiation Research Institute (JASRI) (Proposal No. 2013B1588). The authors appreciate the assistance of Dr. T. Koganezawa (JASRI) with the XRD experiments.

**REFERENCES**

1. Z. Liu, Y. Sun, J. Yuan, H. Wei, X. Huang, L. Han, W. Wang, H. Wang and W Ma, *Adv. Mater.* 2013, **25**, 5772.
2. S. Yao, Z. Chen, F. Li, B. Xu, J. Song, L. Yan, G. Jin, S. Wen, C. Wang, B. Yang and W. Tian, *ACS Appl. Mater. Interfaces*, 2015, **7**, 7146.
3. H.-C. Liao, C.-S. Tsao, T.-H. Lin, M.-H. Jao, C.-M. Chuang, S.-Y. Chang, Y.-C. Huang, Y.-T. Shao, C.-Y. Chen, C.-J. Su, U-Ser Jeng, Y.-F. Chen and W.-F. Su, *ACS nano* 2012, **6**, 1657.
4. Y. Ding, M. Sugaya, Q. Liu, S. Zhou and T. Nozaki, *Nano Energy* 2014, **10**, 322.
5. S. Dayal, N. Kopidakis, D. C. Olson, D. S. Ginley and G. Rumbles, *Nano Lett*. 2010, **10**, 239.
6. S. Ren, N. Zhao, S. C. Crawford, M. Tambe, V. Bulović and S. Gradečak, *Nano Lett*. 2011, **11**, 408.
7. Y. Ding, R. Gresback, Q. Liu, S. Zhou, X. Pi and T. Nozaki, *Nano Energy* 2014, **9**, 25.
8. S. Ren, L.-Y. Chang, S.-K. Lim, J. Zhao, M. Smith, N. Zhao, V. Bulović, M. Bawendi and S. Gradečak, *Nano Lett.* 2011, **11**, 3998.
9. A. Lefrançois, B. Luszczynska, B. Pepin-Donat, C. Lombard, B. Bouthinon, J.-M. Verilhac, M. Gromova, J. F.-Vincent, S. Pouget, *Sci. Rep*. 2015, **5**, 1.
10. A. Abrusci, I-K. Ding, M. Al-Hashimi, T. Segal-Peretz, M. D. McGehee, M. Heeney, G. L. Frey and H. J. Snaith, *Energy Environ. Sci.* 2011, **4**, 3051.
11. Y.-Y. Lin, T.-H. Chu, S.-S. Li, C.-H. Chuang, C.-H. Chang, W.-F. Su, C.-P. Chang, M.-W. Chu and C.-W. Chen, *J. Am. Chem. Soc.* 2009, **131**, 3644.
12. S. D. Oosterhout, M. M. Wienk, S. S. van Bavel, R. Thiedmann, L. J. A. Koster, J. Gilot, J. Loos, V. Schmidt and R. A. J. Janssen, *Nature. Mater.* 2009, **8**, 818.
13. R. Mastria, A. Rizzo, C. Giansante, D. Ballarini, L. Dominici, O. Inganäs and G. Gigli, *J. Phys. Chem. C* 2015, **119**, 14972.
14. L. Martinez, S. Higuchi, A. J. MacLachlan, A. Stavrinadis, N. C. Miller, S. L. Diedenhofen, M. Bernechea, S. Sweetnam, J. Nelson, S. A. Haque, K. Tajima and G. Konstantatos, *Nanoscale* 2014, **6**, 10018.
15. W. S. Yang, J. H. Noh, N. J. Jeon, Y. C. Kim, S. Ryu, J. Seo and S. I. Seok, *Science* 2015, **348**, 1234.
16. S. Mathew, A. Yella, P. Gao, R. H.-Baker, B. F. E. Curchod, N. A.-Astani, I. Tavernelli, U. Rothlisberger, Md. K. Nazeeruddin and M. Grätzel, *Nat. Chem.* 2014, **6**, 242.
17. Z. Yao, M. Zhang, H. Wu, L. Yang, R. Li and P. Wang, *J. Am. Chem. Soc.* 2015, **137**, 3799.

18. J. He, P. Gao, M. Liao, X. Yang, Z. Ying, S. Zhou, J. Ye, Y. Cui, *ACS nano* 2015, **9**, 6522.
19. S. Roland, S. Neubert, S. Albrecht, B. Stannowski, M. Seger, A. Facchetti, R. Schlatmann, B. Rech, D. Neher, *Adv. Mater.* 2015, **27**, 1262.
20. Q. Liu, T. Ohki, D. Liu, H. Sugawara, R. Ishikawa, K. Ueno and H. Shirai, *Nano Energy* 2015, **11**, 260.
21. A. J. Labelle, S. M. Thon, S. Masala, M. M. Adachi, H. Dong, M. Farahani, A. H. Ip, A. Fratalocchi and E. H. Sargent, *Nano Lett.* 2015, **15**, 1101.
22. C.-H. M. Chuang, P. R. Brown, V. Bulović and M. G. Bawendi, *Nat. Mater*. 2014, **13**, 796.
23. C.-C. Chen, W.-H. Chang, K. Yoshimura, K. Ohya, J. You, J. Gao, Z. Honga and Y. Yang, *Adv. Mater.* 2014, **26**, 5670.
24. H. Zhou, Y. Zhang, C. K. Mai, S. D. Collins, G. C. Bazan, T. Q. Nguyen and A. J. Heeger, *Adv. Mater*. 2015, **27**, 1767.
25. J. You, L. Dou, K. Yoshimura, T. Kato, K. Ohya, T. Moriarty, K. Emery, C.-C. Chen, J. Gao, G. Li and Y. Yang, *Nat. Commun*. 2013, **4**, 1446.
26. J. Zhang, Y. Zhang, J. Fang, K. Lu, Z. Wang, W. Ma and Z. Wei, *J. Am. Chem. Soc*. 2015, **137**, 8176.
27. V. Vohra, K. Kawashima, T. Kakara, T. Koganezawa, I. Osaka, K. Takimiya and H. Murata, *Nat. Photon.* 2015, **9**, 403.
28. G. Susanna, L. Salamandra, C. Ciceroni, F. Mura, T.M. Brown, A. Reale, M. Rossi, A. Di Carlo and F. Brunetti, *Sol. Energ. Mat. Sol. Cells* 2015, **134**, 194.
29. B. Kan, M. Li, Q. Zhang, F. Liu, X. Wan, Y. Wang, W. Ni, G. Long, X. Yang, H. Feng, Y. Zuo, M. Zhang, F. Huang, Y. Cao, T. P. Russell and Y. Chen, *J. Am. Chem. Soc.* 2015, **137**, 3886.
30. Y. Liu, C.-C. Chen, Z. Hong, J. Gao, Y. M. Yang, H. Zhou, L. Dou, G. Li and Y. Yang, *Sci. Rep.* 2013, **3**, 3356.
31. K. Gao, L. Li, T. Lai, L. Xiao, Y. Huang, F. Huang, J. Peng, Y. Cao, F. Liu, T. P. Russell, R. A. J. Janssen and X. Peng, *J. Am. Chem. Soc.* 2015, **137**, 7282.
32. C. Y. Liu, Z. C. Holman and U. R. Kortshagen, *Adv. Funct. Mater.* 2010, **20**, 2157−2164.
33. J. H. Parker, D. W. Feldman and M. Ashkin, *Phys. Rev*. 1967, **155**, 712−714.
34. (a) Z. Iqbal, S. Veprek, A. P. Webb and P. Capezzuto, *Solid State Commun*. 1981, **37**, 993−996. (b) H. Xia, Y. L. He, L. C. Wang, W. Zhang, X. N. Liu, X. K. Zhang, D. Feng and H. E. Jackson, *J. Appl. Phys.* 1995, **78**, 6705-1−6705-8. (c) M. N. Islam and S. Kumar, *Appl. Phys. Lett*. 2001, **78**, 715−717.
35. G. Viera, S. Huet and L. Boufendi, *J. Appl. Phys.* 2001, **90**, 4175−4183.
36. R. Mauer, M. Kastler and F. Laquai, *Adv. Funct. Mater.* 2010, **20**, 2085−2092.
37. A. J. Mozer, N. S. Sariciftci, A. Pivrikas, R. Osterbacka, G. Juska, L. Brassat and H. Bassler, *Phys. Rev. B* 2005, **71**, 035214-1−035214-9.
38. S. A. Choulis, Y. Kim, J. Nelson, D. D. C. Bradley, M. Giles, M. Shkunov and I. McCulloch, *Appl. Phys. Lett*. 2004, **85**, 3890−3892.

39. A. J. Mozer and N. S. Sariciftci, *Chem. Phys. Lett.* 2004, **389**, 438−442.
40. X. Shen, V. V. Duzhko and T. P. Russell, *Adv. Energy Mater*. 2013, **3**, 263−270.
41. W. C. Tsoi, D. T. James, J. S. Kim, P. G. Nicholson, C. E. Murphy, D. D. C. Bradley, J. Nelson and J. Kim, *J. Am. Chem. Soc*. 2011, **133**, 9834−9843.
42. S. Wood, J. S. Kim, D. T. James, W. C. Tsoi, C. E. Murphy and J. S. Kim, *J. Chem. Phys.* 2013, **139**, 064901-1−064901-9.
43. Y. Gao and J. K. Grey, *J. Am. Chem. Soc.* 2009, **131**, 9654−9662.
44. Y. Kim, S. Cook, S. M. Tuladhar, S. A. Choulis, J. Nelson, J. R. Durrant, D. D. C. Bradley, M. Giles, I. McCulloch, C. Ha and M. Ree, *Nat. Mater*. 2006, **5**, 197−203.
45. J. Clark, C. Silva, R. H. Friend and F. C. Spano, *Phys. Rev. Lett*. 2007, **98**, 206406-1−206406-4.
46. W. M. Haynes ed., *CRC Handbook of Chemistry and Physics*, 94th Edition. CRC Press, Boca Raton, Florida, 2013.
47. F. Zhang, B. Sun, T. Song, X. Zhu and S. Lee, *Chem. Mater*. 2011, **23**, 2084−2090.
48. L. He, C. Jiang, H. Wang, D. Lai and Rusli, *Appl. Phys. lett*. 2012, **100**, 073503.
49. I. H. Campbell, D. L. Smith, C. J. Neef and J. P. Ferraris, *Appl. Phys. Lett.* 1999, **74**, 2809−2811.
50. P. Cusumoto and S. Gambino, *J. Electron. Mater.* 2008, **37**, 231−239.
51. Y. S. Cho and R. R. Franklin, *Trans. Electr. Electron. Mater.* 2012, **13**, 237−240.
52. C. Y. Liu, Z. C. Holman and U. R. Kortshagen, *Nano Lett*. 2009, **9**, 449−452.
53. P. Favia, E. Voroshazi, P. Heremans and H. Bender, *J. Mater. Sci*. 2013, **48**, 2908−2919.